Heliyon 5 (2019) e02381

Contents lists available at ScienceDirect

Heliyon

journal homepage: www.heliyon.com

Nano-magnetic walnut shell-rice husk for Cd(II) sorption: design and optimization using artificial intelligence and design expert

Lekan Taofeek Popoola *

Unit Operation and Material Science Research Laboratory, Department of Chemical and Petroleum Engineering, Afe Babalola University, Ado-Ekiti, Ekiti State, Nigeria

ARTICLE INFO

Keywords:
Chemical engineering
Environmental science
Cadmium
Walnut shell
Artificial intelligence
Design expert
Rice husk

ABSTRACT

This study attempted to investigate the use of nanomagnetic activated carbon prepared from walnut shell and rice husk wastes for removal of Cd(II) from aqueous solution via application of ANN and design expert as adsorbent preparation design and optimization tools. The novel adsorbent was characterized using SEM, FTIR, EDS and BET. The result from 2-level factorial design expert revealed 78.58% Cd(II) sorption efficiency could be achieved for adsorbent prepared at optimum calcination temperature, calcination time, SS-RH mixing ratio and magnetite loading of 859.20 °C, 2.32 h, 2.54 and 5.56 wt% respectively. Sensitivity analysis by both proposed methodologies revealed calcination temperature as most influential factor in adsorbent preparation. Average relative errors and R^2 values of 1.2931% and 4.806%; and 0.9967 and 0.9055 obtained respectively for developed ANN model with 4-9-1 architecture and 2-level factorial design expert revealed ANN model as better prediction and optimization tool for Cd(II) sorption using NM-WS-RH-AC. Laboratory analysis revealed presence of –OH, –NH and COO^- groups on adsorbent surface; presence of Cd(II) after adsorption; change in adsorbent textural and morphological structure after Cd(II) adsorption; and increase in its surface area and average pore diameter due to magnetization. Average relatively stable desorption strength of 62.74% towards Cd(II) was exhibited by adsorbent for four consecutive cycles using 0.1M HNO_3. Prepared adsorbent is effective in removing Cd(II) from solution than commercial activated carbon with economically viable regeneration attribute.

1. Introduction

It is well-known that the presence of heavy metals in waste water bodies due to natural and anthropogenic activities is extremely dangerous to the lives of humans and aquatic habitants as they interfere with body systems to cause diseases such as liver damage, chronic asthma, diarrhea, kidney congestion, headaches, nausea, vomiting, dermatitis and so on (Ernhart, 1992; Khlifi and Hamza-Chaffai, 2010; Sublet et al., 2003). In the past, findings have shown adsorption as the most prominent and efficient unit operation for the removal of hazardous heavy metals from aqueous solution (Ozcan et al., 2006; Yazdani et al., 2014; Wan Ngah et al., 2011; Popuri et al., 2009; Sahu et al., 2009) as a result of its design and operation simplicity (Bhatnagar and Sillanpaa, 2010); toxic pollutants insensitiveness (Bailey et al., 1999); cost effectiveness (Panneerselvam et al., 2011); high heavy metals sorption efficiency (Yao et al., 2014); negligible sludge formation (Lasheen et al., 2017) and many more. The use of different eco-friendly and low-cost adsorbents from readily available agro-allied waste materials such as *Eucalyptus camaldulensis* Dehn bark (Chatterjee et al., 2011), timber industry waste (Garg, 2005), hen feathers (Mittal, 2006), coconut husk (Tan et al., 2008), Brazilian pine-fruit-shell (Calvete et al., 2009), cotton plant wastes (Tunc et al., 2009), orange peels (AbdurRahman et al., 2013), *Solanum tuberosum* peels (Rehman et al., 2015), grape stalk wastes (Miralles et al., 2010), rice husk-snail shell composite (Popoola et al., 2018), dead *Sargassum* sp. biomass (Ho, 2004), mesoporous fertilizer plant waste (Mall et al., 2006), corncob and barley husk (Robinson, 2002), tamarind wood (Sahu et al., 2009), peanut hull (Tanyildizi, 2011), custard apple peel (Krishnaa and Padma Sree, 2013), coconut tree sawdust (Machado et al., 2011), *Araucaria angustifolia* wastes (Lima et al., 2007), maize bran (Singh et al., 2006), mangosteen shell (Chen et al., 2011), succinylated sugarcane bagasse (Guimarães Gusmão et al., 2012), wheat shell (Bulut and Aydin, 2006), *Ceiba pentandra* hulls (Rao et al., 2006) as adsorbents for heavy metals sorption from aqueous solution to replace expensive and low sorption efficient commercial activated carbon (Gupta et al., 2016) is becoming obsolete in the research world on daily basis. After adsorption process, many of the adsorbents produced from these sources are highly dispersed in the solution which posed great difficulties for their removal. Nevertheless, some of them are difficult to

* Corresponding author.
E-mail address: popoolalekantaofeek@yahoo.com.

https://doi.org/10.1016/j.heliyon.2019.e02381
Received 13 March 2019; Received in revised form 9 July 2019; Accepted 23 August 2019

be recycled for continuous usage.

An ideal adsorbent for heavy metals removal from aqueous solution should exhibit easy removal of adsorbed pollutants from its surface and ability to be recycled over periods before depletion (Sharma et al., 2009; Ali, 2012). The enhanced flexibility function of magnetic particles in removing material from other compounds via attractive magnetic field has called for adsorbent modification with magnetic particles for sorption of heavy metal ions. Synthesized nanomagnetic adsorbents via impregnation and co-precipitation methods (Zainol et al., 2017; Makarchuk et al., 2016) have special features of non-toxicity, chelate complexes formation with ions of heavy metals by ion exchange process or electrostatic interaction, presence of surface functional groups with large active sites, short contact time, recyclability and reusability after separation under magnetic field. In recent times, nanomagnetic activated carbon particles prepared from oil palm (Zainol et al., 2017), chitosan (Ma et al., 2007), tea waste (Panneerselvam et al., 2011), orange peel (Gupta and Nayak, 2012), sugarcane bagasse (Wannahari et al., 2018), modified α-ketoglutaric acid chitosan (Zhou et al., 2009), titanate nanoflowers (Huang et al., 2012), fruit extract of *Momordica cymbalaria* (Swamy et al., 2015) and leaf extract of Cassia didymobotyra (Akhtar et al., 2015) had revealed high sorption efficiency for heavy metals from aqueous solution.

There had been world records of health effects and significance of human exposure to hazardous cadmium in developed countries (Moreno-Castilla et al., 2004; Henretig, 2006). Also, there had been enormous waste generated from walnut shell and rice husk in major cities of Nigeria. In this study, nanomagnetic adsorbent was synthesized for sorption of cadmium ion from solution by impregnation of magnetic particles on calcined particles of walnut shell-rice husk. Both artificial intelligence and design expert were used to design and optimize adsorbent preparation. Four inputs (calcination temperature, calcination time, walnut shell-rice husk mixing ratio and magnetite loading), 9 hidden neurons in hidden layer and one output (cadmium ion sorption efficiency) was the ANN architecture used for adsorbent preparation optimization. The morphology of adsorbent was studied using SEM, FTIR, BET and EDS. Adsorption-desorption strength of adsorbent was investigated for its regeneration and reusability by washing for four consecutive periods with 0.1M HNO_3. Mechanism of adsorptive reaction between Cd(II) and prepared adsorbent was also proposed.

2. Materials and methods

2.1. Materials

Analytical grades of iron (II) chloride [$FeCl_2$], iron (III) chloride [$FeCl_3$], sodium hydroxide [NaOH], potassium hydroxide [KOH] and trihydrates of cadmium nitrate [$Cd(NO_3)_2.3H_2O$] were purchased from TopJ Scientific, Ajilosun Road, Ado-Ekiti, Ekiti State, Nigeria. Rice husk was obtained as remnants from Lafenwa market, Abeokuta, Ogun State, Nigeria while shells of walnut eaten by the researcher bought from local sellers in Ibadan, Oyo State, Nigeria between July–October, 2018 were stored for research purpose.

2.2. Preparation of Cd(II) adsorbate solution

One gram of Cd(II) salt was dissolved in 1 L of distilled water to form simulated stock solutions in 1000 mL round bottom flask. Salt solution with initial concentration of 50 mg/L was prepared in 200 mL conical flasks for batch adsorption process.

2.3. Nanomagnetic walnut shell-rice husk activated carbon preparation

The method adopted for pre-treatment and walnut shell-rice husk activated carbon (WS-RH-AC) preparation by calcination have been presented elsewhere (Popoola et al., 2018). The method of chemical co-deposition presented by Novopashin et al. (2015) was applied to prepare the magnetite in magnetic fluid form which was stabilized by using citric acid. The magnetite was impregnated into the activated carbon produced via calcination of walnut shell-rice husk to form nanomagnetic walnut shell-rice husk activated carbon (NM-WS-RH-AC). The purpose of calcination is to enhance creation of more cavities for adsorption of heavy metals via evacuation of adsorbed gases (Popoola et al., 2018) which is not necessary for magnetic particles due to their non-porous (Sadegh et al., 2017; Nassar, 2010; Fan et al., 2012) and flexibility (Zainol et al., 2017) attributes. The weight percent of impregnated magnetite was varied with WS-RH-AC based on the coded levels of the adsorbent preparation conditions (calcination temperature, walnut shell-rice husk mixing ratio, calcination time and magnetite loading) obtained from 2^k factorial experimental design of Design Expert 7.0.0 software presented in Table 1. To obtain homogenized and thoroughly mixed NM-WS-RH-AC, the mixture was mechanically stirred for 45 min and then separated with aid of magnetic filter using magnetic induction of 58 mT external magnetic field. The obtained residue was then dried at a temperature of 140 °C in an oven for 1 h.

2.4. Batch adsorption process

A temperature-controlled magnetic heat stirrer (Stuart heat-stirrer SB162) was used to study the batch adsorption process while concentration of Cd^{2+} was measured via atomic absorption spectrometer (AAS Buck Scientific 210 VGP). 0.5 g of NM-WS-RH-AC was mixed with 50 mL of Cd (II) salt in a 100-mL flask. Each batch adsorption process was conducted at 30 °C and 120 revolutions per minute at a contact time of 45 min to study the equilibrium attainment. NM-WS-RH-AC was separated from Cd (II) salt solution after adsorption using 10mm filter paper. Concentrations were measured in quadruplets at dilution factor of 50 such that the average values were recorded for the final concentration. The adsorption capacity of NM-WS-RH-AC, q_e (mg/g) and Cd^{2+} sorption efficiency at equilibrium were measured using Eqs. (1) and (2) respectively.

$$q_e = (C_o - C_e)\frac{V}{W} \tag{1}$$

$$\%\ \ Cd^{2+}\ \ \text{Sorption} = \frac{(C_o - C_e)}{C_o} \times 100\% \tag{2}$$

where C_o and C_e are initial and final concentrations of Pb^{2+} and Cd^{2+} (mg/L), V is is the volume of solution (L) and W is the weight of adsorbent (g).

2.5. Design of experiments for adsorbent preparation and optimization

The optimization goals include (1) experimental design and (2) maximization of NM-WS-RH-AC adsorbent preparation conditions that give optimum sorption of Cd^{2+} from aqueous solution using both artificial intelligence neural network and 2-level factorial design of Design Expert 7.0.0 to predict the outputs.

2.5.1. 2-Level factorial design

In this, the number of experiments required to determine optimum

Table 1
NM-WS-RH-AC preparation factor coding and variable ranges using 2-level factorial design.

Independent Variables	Factor	Unit	Low Level (-1)	High level (+1)
Calcination Temperature	X_1	(°C)	600	1000
Calcination Time	X_2	(hr)	1	5
Walnut Shell-Rice Husk Mixing Ratio	X_3	-	1	5
Magnetite Loading	X_4	(wt %)	2	10

process variables is varied over two levels (low and high) unlike central composite design where experimental values are varied over five levels (axial points, factorial points and center point). Thus, minimising the number of experiments to be conducted for optimum process variables determination to study variables interaction with one another. For this study, calcination temperature, calcination time, walnut shell-rice husk mixing ratio and magnetite loading were the process independent variables investigated with percent of Cd^{2+} sorption being the desired outputs to maximize NM-WS-RH-AC adsorbent preparation conditions. Table 1 presents NM-WS-RH-AC preparation factor coding and variable ranges. Sum total of 16 experimental runs were conducted for NM-WS-RH-AC preparation and Cd^{2+} sorption optimization based on 2^k factorial design with four ($2^4 = 16$) process variables.

2.5.2. Artificial neural network (ANN)

An ANN is capable of learning relationships between given sets of input and output data via changing the weights called training using back propagation training algorithm (Popoola, 2016). Superiority advantages of ANN over other predictive tools have been presented elsewhere (Singh et al., 2017). In this study, neural network architecture with configuration 4-9-1 (Nasr et al., 2012) was used to optimize NM-WS-RH-AC preparation conditions as shown in Fig. 1 via prediction of Cd^{2+} removal efficiency. ANN configuration for optimization of NM-WS-RH-AC preparation conditions comprises of input layer with four experimental factors (calcination temperature, calcination time, walnut shell-rice husk mixing ratio and magnetite loading), hidden layer with 9 neurons (to avoid network overfitting) and output layer for the response (Cd^{2+} sorption efficiency). The networks' weights and biases were adjusted iteratively for mean squared error (MSE) minimization such that 60%, 30% and 10% of the input and target vectors were respectively used for training, validation and testing. The weight and bias values were updated during training using the generalized form multilayer perceptron back-propagation algorithm stated as Eq. (3) while hyperbolic tangent sigmoid "tansig" function stated as Eq. (4) was used as hidden layer transfer function which limits the output between -1 and +1. The output signal y_k generated by neuron k of the ANN is given as Eq. (5). For function fitting in the output layer, "purlin" transfer function presented in Eq. (6) was used such that output was generated in the range of $-\infty$ to $+\infty$.

$$w_{ij}^{k+1} = w_{ij}^{k} + \eta\delta_j^k I_i f'(s) \tag{3}$$

$$\varphi(x) = 2\left(1 + \exp^{-2x}\right)^{-1} - 1 \qquad -1 \le \varphi(x) \le 1 \tag{4}$$

$$y_k = \varphi\left(\sum_{j=1}^{m} W_{kj}.x_j + b_k\right) \tag{5}$$

$$\varphi(x) = x \qquad -\infty < \varphi(x) < +\infty \tag{6}$$

where W_{ij}^k = connection weights from unit i in layer k to unit j in layer $k+1$, η = learning rate, δ_j^k = signal error, I_i = input vector to the networks, $f'(s)$ = networks transfer function derivative, s = sum of all the weights, y_k = output signal, φ = activation function, m = total number of inputs to the neuron, j = input, W_{kj} = synaptic weight of input j for neuron k, x_j = input signal, b_k = bias value of neuron k.

2.6. NM-WS-RH-AC adsorbent characterization

The NM-WS-RH-AC adsorbent that gives optimum removal efficiency of Cd^{2+} from aqueous solution was characterized before and after adsorption process. The existing chemical bonding and functional groups of NM-WS-RH-AC was observed over the wavelength range of 300–4000 cm^{-1} using FTIR spectrometer (Nicolet iS10 FT-IR Spectrometer) and

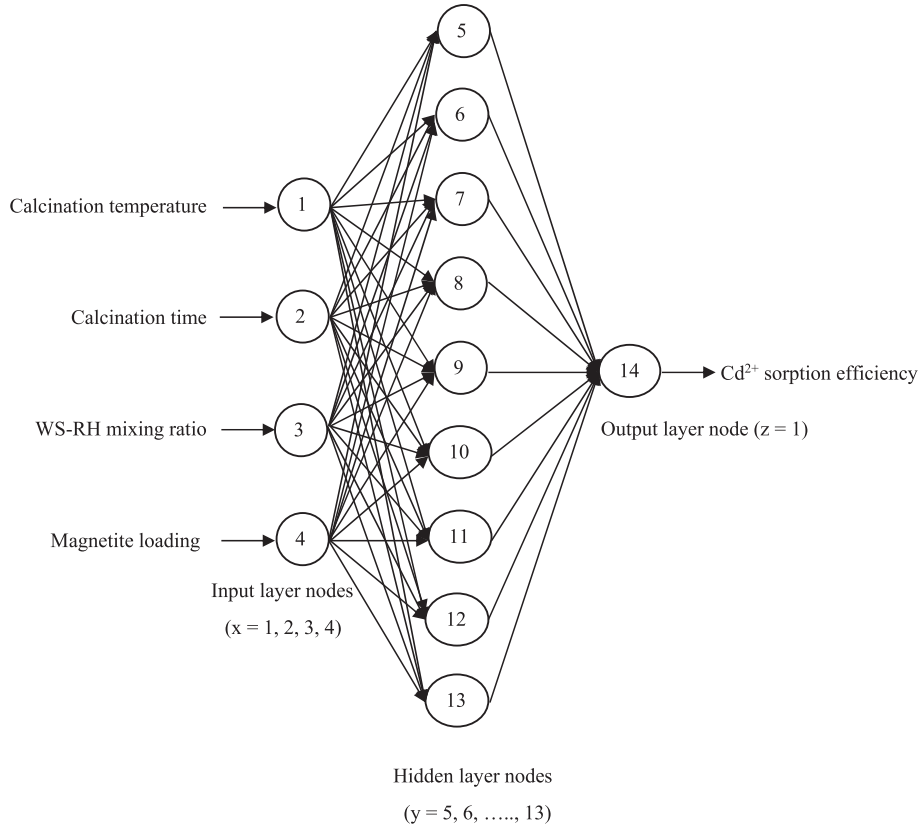

Fig. 1. Artificial neural network architecture with configuration of 4-9-1 for NM-WS-RH-AC preparation conditions optimization to predict Cd^{2+} removal efficiency using calcination temperature, calcination time, walnut shell-rice husk mixing ratio and magnetite loading as experimental input parameters.

obtained spectra were analyzed further. The adsorbent's elemental analysis and structural morphology was investigated using scanning electron microscope (SEM/EDX-JEOL-JSM 7600F) at 5000×, 15 kV under high-vacuum evaporation of sample deposition methodology. In order to examine the effect of calcination and magnetization on surface area, pore volume and pore diameter of mixed walnut shell-rice husk, Brunauer-Emmett-Teller method was executed by using a Quantachrome Autosorb instrument (Nova 11.03A, USA version). This was achieved based on physical nitrogen adsorption principle at 77 K.

2.7. NM-WS-RH-AC regeneration and reusability

The sorption strength of prepared NM-WS-RH-AC for Cd^{2+} from aqueous solution was thoroughly investigated using 0.1M HNO_3. After the first sorption process, distilled water at 7.0 pH was used to thoroughly wash the NM-WS-RH-AC adsorbent after which it was dried at 80 °C for 6 h and reused for four consecutive times in order to affirm its reusability capacity for Cd^{2+} sorption from aqueous solution. The method of calculating desorption efficiency of prepared adsorbent presented by Giri et al. (2011) was adopted.

3. Results and discussion

3.1. 2-Level factorial design expert for NM-WS-RH-AC preparation conditions

The 2^k factorial level of design expert was instrumental in developing mathematical model to predict Cd(II) sorption, statistical analysis of data, studying of model factors contributory effects and optimum numerical point prediction of process variables for NM-WS-RH-AC preparation required for optimum Cd(II) sorption from aqueous solution.

3.1.1. Model development and statistical analysis

In order to determine NM-WS-RH-AC preparation conditions (calcination temperature, calcination time, SS-RH mixing ratio and magnetite loading) that gives optimum percent Cd^{2+} sorption from aqueous solution (response), 16 experimental runs were generated using the 2^k factorial level of design expert as shown in Table 2. It was observed that NM-WS-RH-AC14 prepared at calcination temperature, calcination time, SS-RH mixing ratio and magnetite loading of 1000 °C, 5 h, 1.00 and 10wt % respectively gave the maximum Cd^{2+} percent sorption of 96.9938% from aqueous solution while minimum percent Cd^{2+} removal of 43.7617% was observed for NM-WS-RH-AC15 prepared at calcination temperature, calcination time, SS-RH mixing ratio and magnetite loading of 600 °C, 1 h, 5.00 and 2wt% respectively. This revealed sorption of Cd^{2+} from aqueous solution was favoured at optimum calcination temperature, calcination time and magnetite loading with negligible influence of walnut shell-rice husk mixing ratio (Popoola, 2019). This is also evident in NM-WS-RH-AC8 which gave 66.8251% at respective minimum calcination temperature, calcination time and magnetite loading of 600 °C, 1 h and 2wt% as compared to NM-WS-RH-AC15 with lowest sorption efficiency even at maximum walnut shell-rice husk mixing ratio of 5. This shows the negligible influence of SS-RH mixing ratio in the adsorption process.

Eq. (7) presents the regression model linking both dependent and independent variables together based on coded factors X_1, X_2, X_3 and X_4. Table 3 presents the Type III ANOVA results to validate the authenticity of this developed quadratic model equation as suggested by the 2-level factorial design. The result revealed the significance of the model as its recorded respective F-value and probability value (Prob˃F) of 7.9840 and 0.02449 (Popoola, 2019). The p-values of X_1, X_2, X_4, X_1X_2, X_1X_4 and X_2X_4 being less than 0.05 also revealed the significance of these factors in the developed model while other model terms were considered insignificant.

Table 2
2^k factorial level experimental design for NM-WS-RH-AC preparation conditions.

Adsorbent Code	Calcination Temp. (°C) X_1	Calcination Time (hr) X_2	SS-RH Mixing ratio X_3	Magnetite loading (wt%) X4	Adsorbent Capacity (mg/g)	Cd^{2+} Sorption efficiency (%)		
						Exp.	Predicted	
							2^k-factorial Design	Absolute Error (%)
NM-WS-RH-AC1	600.00	1.00	1.00	10.00	126.738	55.3172	58.75089	6.207
NM-WS-RH-AC2	1000.00	5.00	5.00	2.00	168.236	79.4007	73.21679	7.788
NM-WS-RH-AC3	1000.00	5.00	1.00	2.00	129.104	58.2315	61.37179	5.393
NM-WS-RH-AC4	600.00	1.00	5.00	10.00	103.305	72.5418	68.74394	5.235
NM-WS-RH-AC5	600.00	5.00	1.00	2.00	151.004	77.7723	84.08097	8.112
NM-WS-RH-AC6	1000.00	5.00	5.00	10.00	177.238	83.4069	81.12487	2.736
NM-WS-RH-AC7	1000.00	1.00	5.00	10.00	165.413	81.2532	78.91269	2.881
NM-WS-RH-AC8	600.00	1.00	1.00	2.00	132.541	66.8251	78.79934	17.919
NM-WS-RH-AC9	1000.00	1.00	1.00	2.00	168.739	84.6324	82.10544	2.986
NM-WS-RH-AC10	600.00	5.00	1.00	10.00	137.335	59.6318	57.03472	4.355
NM-WS-RH-AC11	600.00	5.00	5.00	2.00	141.992	68.4517	69.12837	0.989
NM-WS-RH-AC12	1000.00	1.00	5.00	2.00	172.387	87.2381	85.70969	1.752
NM-WS-RH-AC13	1000.00	1.00	1.00	10.00	178.441	91.3452	93.85459	2.747
NM-WS-RH-AC14	1000.00	5.00	1.00	10.00	184.164	96.9938	97.54227	0.565
NM-WS-RH-AC15	600.00	1.00	5.00	2.00	127.527	43.7617	46.37007	5.960
NM-WS-RH-AC16	600.00	5.00	5.00	10.00	141.518	73.9835	73.04044	1.275
Average Absolute Error								4.806

Table 3
ANOVA (Type III) result of the 2^k factorial design for NM-WS-RH-AC preparation conditions.

Source	Sum of Squares	Df	Mean Square	F-Value	Prob > F
Model	1909.053	10	190.9053	7.98402	0.02449
X_1	1299.904	1	1299.904	5.436441	0.0171
X_2	13.98293	1	13.98293	5.8479	0.03185
X_3	0.031657	1	0.031657	0.000132	0.9913
X_4	144.961	1	144.961	6.06254	0.04714
X_1X_2	287.5526	1	287.5526	4.202599	0.03228
X_1X_3	0.051042	1	0.051042	0.000213	0.5889
X_1X_4	94.24963	1	94.24963	2.39417	0.04577
X_2X_3	42.05036	1	42.05036	0.175863	0.6924
X_2X_4	9.241144	1	9.241144	3.8648	0.02519
X_3X_4	17.02903	1	17.02903	0.071219	0.8002
Residual	1195.546	5	239.1093	-	-
Cor Total	3104.599	15	-	-	-

$R^2 = 0.9055$; Adj-$R^2 = 0.8281$; Std. Dev. = 4.4182; Conf. Level = 95%

Nevertheless, close to unity R^2 value of 0.9055, lower standard deviation value of 4.4182 and confidence level of 95% suggest developed model exactness. Fig. 2(a) represents the plot of experimental and predicted Cd^{2+} sorption by NM-WS-RH-AC. Thus, the developed model is a true representation of 90.55% of the total variation in the experimental Cd(II) sorption attributed to independent variables considered in this study.as revealed by the R^2 value being 0.9055. Fig. 2(b) also confirms the uniqueness of the model as all presented errors at various points of the calcination temperature and time were between 0.292 ≤ design standard error ≤ 0.458.

$$Cd^{2+}\ \text{Sorption}\ (\%) = +75.05 + 7.76X_1 - 0.32X_2 + 1.21X_3 + 1.76X_4 - 2.99X_1X_2 - 1.19X_1X_3 + 3.68X_1X_4 + 0.37X_2X_3 + 2.01X_2X_4 - 0.22X_3X_4 \quad (7)$$

3.1.2. Contributory effects of model factors

Fig. 3(a) depicts the Pareto chart showing the percent contribution of each model factor as obtained from the effect tools box of 2^k factorial level design expert to the Cd(II) sorption efficiency of the prepared NM-WS-RH-AC. The order of percent contributory effect of main factors to NM-WS-RH-AC efficiency to remove Cd(II) from aqueous solution was calcination temperature (X_1)˃magnetite loading (X_4)˃calcination time (X_2)˃walnut shell-rice husk mixing ratio (X_3) having values 44.87% ˃13.24%˃7.04%˃1.64%. This shows increasing calcination temperature from 600 °C to 1000 °C during NM-WS-RH-AC preparation has a great influence on its Cd(II) adsorption capability. Adsorptive efficiency of adsorbent has been shown to increase with increase in calcination temperature as more water vapours are evaporated thus, creating more pores for heavy metal adsorption onto its surface (Popoola, 2019). This revelation was also supported by results of adsorptive efficiency of various NM-WS-RH-AC towards Cd(II) prepared at different conditions (presented in Table 2) as those prepared at 1000 °C have higher Cd(II) adsorption efficiency than those prepared at 600 °C. The positive contributory effects of magnetite loading (Panneerselvam et al., 2011) and calcination time (Chen et al., 2011) on adsorptive efficiency of locally produced adsorbents towards heavy metal have been presented elsewhere. Also, the 3D-response surface cubic plot (shown in Fig. 3b) depicts increase in Cd(II) uptake from aqueous solution as calcination temperature (X_1) and calcination time (X_2) increases from 1-5 h and 600–1000 °C respectively while SS-RH mixing ratio and magnetite loading were kept at centre point with respective values of 3.00 and 6.00. In conclusion, contributory order of factors effect is evident in NM-WS-RH-AC14 (shown in Table 2) prepared at 1000 °C calcination temperature, 5 h calcination time, 1 SS-RH mixing ratio and 10wt% magnetite loading which gave the highest experimental Cd(II) adsorption efficiency with lowest SS-RH mixing ratio.

3.1.3. Numerical optimization point prediction of NM-WS-RH-AC process variables

Table 4 presents the optimum point predicted by the 2^k factorial level design expert with the objective of maximizing Cd(II) sorption from aqueous solution subject to minimising process variables (preparation conditions) of NM-WS-RH-AC. At these points, an experimental run was conducted to check the efficiency of predicted model (Equation 7). The percentage of Cd(II) from aqueous solution using NM-WS-RH-AC prepared at calcination temperature, calcination time, SS-RH mixing ratio and magnetite loading of 859.20 °C, 2.32 h, 2.54 and 5.56 wt% respectively was 78.58%. This shows good agreement between experimental and predicted results at optimum points with an approximate relative error of 2.91%. This indicates maximum Cd(II) sorption could be attained at NM-WS-RH-AC optimum preparation conditions.

3.2. Artificial neural network

3.2.1. Network weights and biases adjustment

In order to improve the performance of the network, adaption of its adjustable parameters (weights and biases) during ANN model training is required for its output to match with the target value. The magnitude of performance gradient being lower than $1e^{-5}$ implies completion of training step (Popoola and Susu, 2014).

In this study, the network architecture has four, nine and one neurons in input, hidden and output layers respectively such that each element present in the 4-length input vector ($P_{4\times1}$) was connected to each neuron present in the 9-length hidden layer via a 9×4 weight matrix ($W_{9\times4}$). This makes the sum of the weighted inputs to be $\sum W_{9\times4}.P_{4\times1}$ such that the

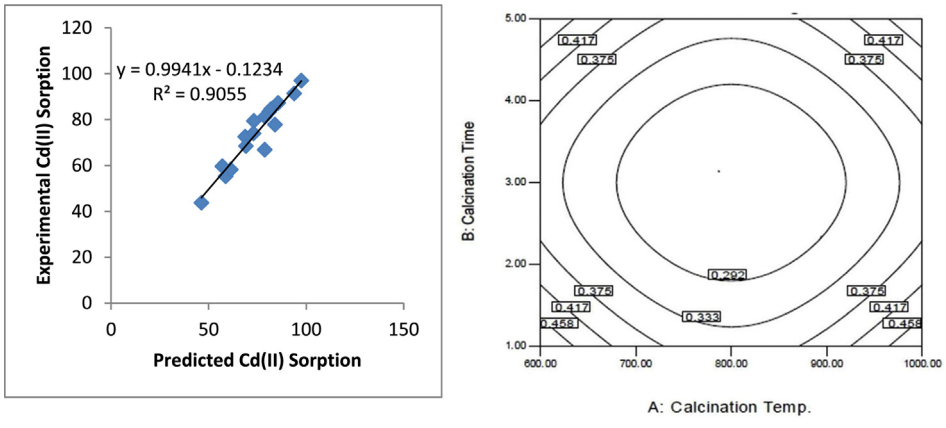

(a) (b)

Fig. 2. (a) Percent values of experimental against predicted Cd(II) sorption (b) Standard error contour of 2^k factorial design for Cd(II) sorption using NM-WS-RH-AC.

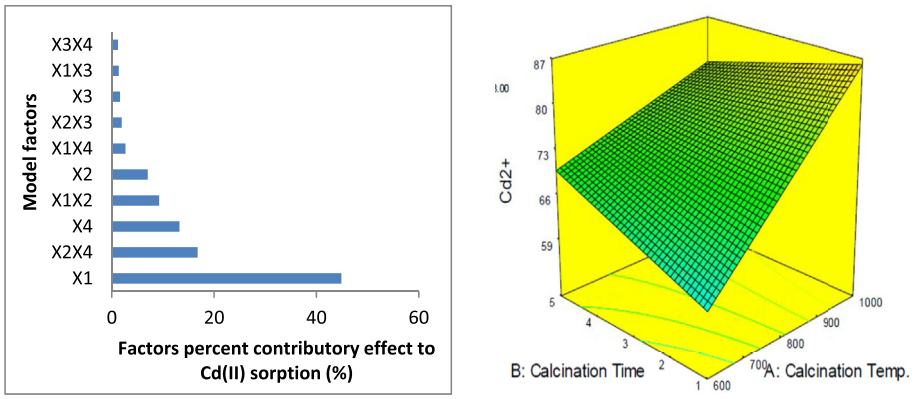

(a) (b)

Fig. 3. (a) Pareto chart of model factors contribution percent (b) 3D surface plot depicting calcination temperature and time effects on Cd(II) adsorption onto NM-WS-RH-AC.

Table 4
Optimum point prediction and experimental result of percent Cd(II) sorption at minimized NM–SS– RH-AC preparation condition using 2^k factorial level design expert.

Parameter	Predicted Optimum Value	% Cd(II) Sorption	
		Predicted	Experimental
Calcination Temperature (X_1)	859.20 °C	76.36%	78.58%
Calcination Time (X_2)	2.32 h	-	-
SS-RH Mixing Ratio (X_3)	2.54	-	-
Magnetite loading (X_4)	5.56 wt%	-	-

addition of a 9-length bias ($b_{9\times1}$) gives $u_{9\times1} = \sum W_{9\times4}.P_{4\times1} + b_{9\times1}$. The summed net input was then transformed via "tansig" transfer function to the hidden layer to have $f(u) = \text{tansig}\,(\sum W_{9\times4}.P_{4\times1} + b_{9\times1})$. In between the hidden layer and output layer, each neuron present in the vector of 9-length hidden layer ($P_{9\times1}$) was connected to the one-neuron output layer via a 1×9 weight matrix ($W_{1\times9}$). The input weighted sum gives $\sum W_{1\times9}.P_{9\times1}$ such that the addition of a 1-length bias ($b_{1\times1}$) gives $u_{1\times1} = \sum W_{1\times9}.P_{9\times1} + b_{1\times1}$. The summed net input was then transformed via "purlin" transfer function to the output layer to give $f(u) = \text{purlin}\,(u_{1\times1} = \sum W_{1\times9}.P_{9\times1} + b_{1\times1})$.

3.2.2. Performances of training and validation steps

The network training process was terminated after the validation check number and performance gradient magnitude of 7 and 0.2618 were respectively attained. The gradient magnitude greater than $1e^{-5}$ least error level is an implication of best validation performance. Table 5 presents values of weights connection ($W_{9\times4}$ and $W_{1\times9}$) and threshold levels ($b_{9\times1}$ and $b_{1\times1}$) at these conditions where minimum square error was achieved on the validation set. These neural network biases and weights were then used to develop best-fit outputs for training data.

3.2.3. Sensitivity analysis of model factors

The contributory effect (sensitivity analysis) of each of the process variables (calcination temperature, calcination time, walnut shell-rice husk mixing ratio and magnetite loading) on the sorption efficiency of prepared NM-WS-RH-AC towards Cd(II) was investigated using the proposed optimal ANN model weights presented in Table 5. To achieve this, Eq. (8) which employs network's connection weights partitioning methodology (Garson, 1991) was used while date arrangement and sensitivity analysis computation has been presented elsewhere (Ranasinghe et al., 2017).

$$S_j = \frac{\sum_{y=1}^{y=N_h}\left(\left(\frac{|W_{jy}^{ih}|}{\sum_{x=1}^{N_i}|W_{xy}^{ih}|}\right)\times\left|W_{yz}^{ho}\right|\right)}{\sum_{x=1}^{x=N_i}\left(\sum_{y=1}^{y=N_h}\left(\frac{|W_{xy}^{ih}|}{\sum_{x=1}^{N_i}|W_{xy}^{ih}|}\right)\times\left|W_{yz}^{ho}\right|\right)} \quad (8)$$

where S_j is the jth input variable relative sensitivity on output variable, W stands for connection weight, N_h is the numbers of hidden neurons and N_i represents number of input neurons. The subscripts 'x', 'y' and 'z'

Table 5
Proposed ANN model weights and threshold levels.

Hidden layer node	Input layer weight from node i to node j in hidden layer for $W_{9\times4}$ matrix				Hidden layer threshold ($b_{9\times1}$)
	x = 1	x = 2	x = 3	x = 4	
y = 5	-0.0774	-0.3392	-2.7002	-1.6919	-3.7065
y = 6	1.2317	-4.6182	-0.8631	-0.4106	-0.1927
y = 7	-4.6302	0.6910	-4.4379	2.7285	2.416
y = 8	9.5182	3.2164	1.4178	-3.4201	-1.5204
y = 9	-0.5378	-0.7231	-0.0498	1.3432	-5.5303
y = 10	-0.6182	1.2871	2.7875	-0.7554	-0.9224
y = 11	3.7192	-1.4198	1.8248	3.5480	-2.5443
y = 12	1.3291	7.1828	-1.7103	-1.0934	2.9476
y = 13	-1.7834	-0.2937	-3.6041	5.6183	6.2630

Output layer node	Hidden layer weight from node j to node k in output layer for $W_{1\times9}$ matrix									Output layer threshold ($b_{1\times1}$)
	y = 5	y = 6	y = 7	y = 8	y = 9	y = 10	y = 11	y = 12	y = 13	
z = 14	-2.9253	0.1868	-0.2391	-0.2925	0.9889	-2.7329	0.0150	-0.2246	-0.2252	-0.8686

Note: x = input layer node, y = hidden layer node, z = output layer node.

represent input, hidden and output neurons respectively while superscripts '*i*', '*h*' and '*o*' are input, hidden and output layers respectively.

Fig. 4 presents the percent relative significance of the input variables for NM-WS-RH-AC preparation which enhanced its adsorptive efficiency for Cd(II) removal from aqueous solution. The order of significance was calcination temperature, magnetite loading, calcination time and SS-RH mixing ratio with respective percent contributory effect of 44.82%, 28.14%, 21.37% and 5.67%. From these, the calcination temperature was the most significant factor among the examined process variables exhibiting 44.82% adsorption contributory effect. Previous studies have also revealed the importance of temperature in adsorbent preparation (Panneerselvam et al., 2011; Tanyildizi, 2011). Also, similar order of variables significance was obtained for variables contributory effect studied using 2-level factorial design expert. This results revealed that none of the variables examined could be neglected from this study and proposed ANN model is a good representation of Cd(II) sorption from aqueous solution using NM-WS-RH-AC prepared within specified process variables ranges.

3.2.4. Developed ANN model testing, regression and optimization

Table 6 presents the results of the testing step of developed ANN model in order to check for its efficacy in predicting minimum NM-WS-RH-AC preparation conditions that give optimum Cd(II) sorption from aqueous solution. For comparative purpose, random input vectors from 2-level factorial were used as input variables for the ANN model. The average absolute error obtained was 1.2931% for Cd(II) sorption efficiency as compared to 4.806% obtained when 2-level factorial experimental design was used as the design and optimization tool. This reveals ANN model as better prediction tool than 2-level factorial design expert for Cd(II) sorption using NM-WS-RH-AC. A lower average absolute error implies better accuracy which is an indication of better prediction. Though this research work *is first of its kind* as none had used artificial intelligence and design expert as comparative tools for Cd(II) sorption from aqueous solution using activated carbon prepared from nano-magnetised walnut shell-rice husk, previous studies have proved ANN as better design and optimization tool (Popoola, 2016; Khataee and Kasiri, 2011). The regression plot (testing result) of target (experimental) against predicted (ANN) output for the Cd(II) removal efficiency by NM-WS-RH-AC using ANN architecture of 4-9-1 (shown in Fig. 5) revealed R^2 value of 0.9967. This shows only 0.33% of the response total variability could not be explained by the ANN model indicating excellent performance efficiency of developed ANN to be 99.67%. All these are evident enough to prove that the developed ANN was a better response prediction tool.

3.3. NM-WS-RH-AC characterization

3.3.1. SEM

The scanning electron micrographs of NM-WS-RH-AC prepared at optimum conditions (calcination temperature = 859.20 °C, calcination time = 2.32 h, WS-RH mixing ratio = 2.54 and magnetite loading = 5.56 wt%) predicted by two-level factorial design expert before and after Cd(II) sorption are presented in Fig. 6. The SEM image (Fig. 6a) revealed formation of pores having unevenly-distributed particle size and shape with high deposition of magnetite on the adsorbent surface before Cd(II) adsorption. These are special features that would enhance easy solutes adsorption and percolation onto active pores on adsorbent surface (Krishna Mohan et al., 2017). Similar studies have also obtained similar SEM image of nano-magnetic adsorbent before adsorption (Giri et al., 2011; Wannahari et al., 2018). However, a change in the textural and morphological structure of the used NM-WS-RH-AC was observed after Cd(II) sorption from aqueous solution as presented in Fig. 6b showing blockage of pores with reduction in their number, spaces and surface area. These changes revealed adsorption of Cd(II) onto NM-WS-RH-AC surface and pores.

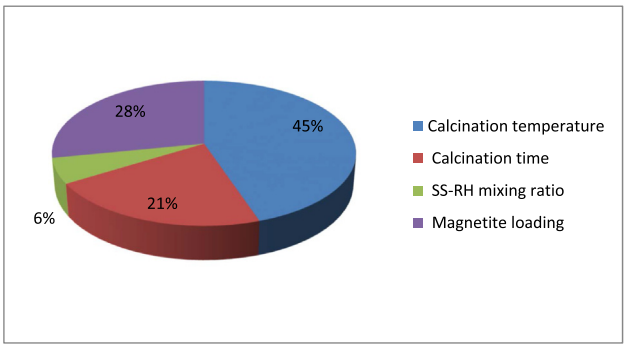

Fig. 4. Sensitivity analysis of ANN input variables significance on NM-WS-RH-AC efficiency for Cd(II) sorption from aqueous solution.

3.3.2. FTIR

Fig. 7 presents the Fourier-Transform-Infrared spectra of NM-WS-RH-AC adsorbent before and after Cd(II) sorption studied over wavelength range of 300–4300nm. This was executed in order to know (i) active functional groups on adsorbent's surface that have enhanced Cd(II) sorption from aqueous solution (ii) bonding structures present in adsorbent and (iii) adsorption mechanism between adsorbent and Cd(II) solution. Shift of broad peaks from 3428, 1814 and 1446 cm^{-1} before adsorption to 3462, 1758 and 1428 cm^{-1} after adsorption indicates bending vibration of –OH (Cao et al., 2014), stretching vibration of –NH and carbonyl stretching of COO^- (Panneerselvam et al., 2011) functional groups respectively. These indicate adsorption of Cd(II) onto NM-WS-RH-AC surface by formation of hydrogen bond involving –OH, –NH and COO^-. The most affirmative proof of Cd(II) sorption onto NM-WS-RH-AC surface was the appearance of sharp broad peaks present at 2048, 3284 and 3764 cm^{-1} on the IR spectrum after adsorption pertaining to cadmium presence which are missing on IR spectrum before adsorption.

3.3.3. EDS

The result of energy dispersive spectroscopy analysis showing elemental weight percent of adsorbent before and after Cd(II) adsorption from aqueous is presented in Table 7. The larger weight percent of calcium (13.21%) and silicon (21.20%) could be traced to walnut shell and rice husk respectively (Korotkova et al., 2016) while presence of iron (38.85%) is a strong evidence of their magnetization before Cd(II) adsorption. The following observations are strong evidence of Cd(II) sorption onto NM-WS-RH-AC (1) changes in the weight percent of adsorbent elemental composition (Popoola, 2019) (2) reduction in oxygen and hydrogen content implies H^+ and OH^- reaction has occurred on adsorbent surface and (3) presence of cadmium in the adsorbent (found missing before adsorption) after adsorption.

3.3.4. BET

A comparison of pore volume, surface area and pore diameter of raw walnut shell-rice husk (RWS-RH), calcinated walnut shell-rice husk (CWS-RH) and nanomagnetic walnut shell-rice husk activated carbon (NM-WS-RH-AC) executed using Brunauer-Emmett-Teller analysis with commercial activated carbon (CAC) is presented in Table 8. The CWS-RH and NM-WS-RH-AC were prepared at predicted optimum operating conditions (X_1 = 859.20 °C, X_2 = 2.32 h, X_3 = 2.54 and X_4 = 5.56 wt%) suggested by 2^k factorial level design expert. The CWS-RH was prepared without magnetite loading. The contributory effects of calcination temperature and calcination time were manifested as surface area, total pore volume and average pore diameter increased from 38.08 m^2g, 0.0073 cm^2g and 2.77 Å for RWS-RH to 94.54 m^2/g, 0.0932 cm^2/g and 3.31 Å for CWS-RH respectively (Popoola, 2019). Magnetization of CWS-RH influenced increase in its surface area and average pore diameter from 94.54 m^2/g and 3.31 Å to 126.72 m^2/g and 4.18 Å for NM-WS-RH-AC

Table 6
Testing results of developed ANN model using randomly picked experimental runs.

Adsorbent Code	Calcination Temp. (°C) X_1	Calcination Time (hr) X_2	SS-RH Mixing ratio X_3	Magnetite loading (wt %) X4	Adsorbent Capacity (mg/g)	Cd^{2+} Sorption efficiency (%)		
						Exp.	Predicted	
							ANN	Absolute Error (%)
NM-WS-RH-AC1	600.00	1.00	1.00	10.00	126.738	55.3172	54.6232	1.2546
NM-WS-RH-AC3	1000.00	5.00	1.00	2.00	129.104	58.2315	60.0128	3.0590
NM-WS-RH-AC8	600.00	1.00	1.00	2.00	132.541	66.8251	64.9045	2.8741
NM-WS-RH-AC13	1000.00	1.00	1.00	10.00	178.441	91.3452	91.4659	0.1321
NM-WS-RH-AC14	1000.00	5.00	1.00	10.00	184.164	96.9938	96.6371	0.3678
NM-WS-RH-AC15	600.00	1.00	5.00	2.00	127.527	43.7617	43.7307	0.0708
Average Absolute Error								1.2931

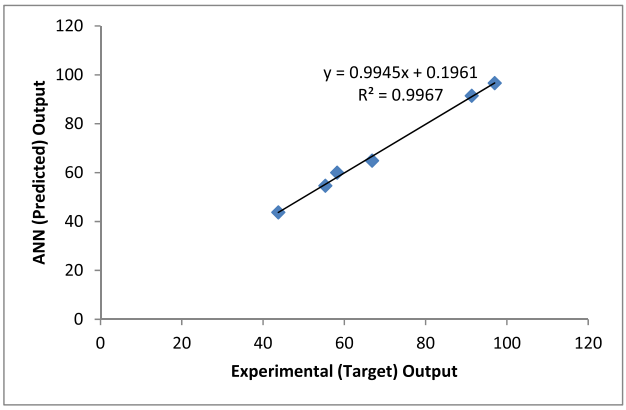

Fig. 5. Regression plot of predicted output against experimental output for Cd(II) sorption efficiency by NM-WS-RH-AC using 4-9-1 ANN architecture.

respectively. This could be attributed to magnetic particles dispersion at high level on CWS-RH surface having a specific surface area (Park et al., 2011). Similar studies have also revealed increase in surface area of parent materials after magnetic particles impregnation (Hu et al., 2011; Panneerselvam et al., 2011; Zainol et al., 2014). However, a slight reduction in total pore volume from 0.0932 cm^2/g for CWS-RH to 0.0811 cm^2/g for NM-WS-RH-AC was observed which could result from smoother texture of NM-WS-RH-AC surface after impregnation of magnetite (Idan et al., 2018). Conclusively, the prepared NM-WS-RH-AC revealed better textural properties and porous structure than CAC. Table 9 presents textural properties of previous nanomagnetic activated carbons of parent materials used as adsorbent as compared with present study.

3.4. NM-WS-RH-AC regeneration and reuse

The adsorption-desorption cycles of NM-WS-RH-AC prepared at 2^k factorial level design expert predicted optimum operating conditions (X_1 = 859.20 °C, X_2 = 2.32 h, X_3 = 2.54 and X_4 = 5.56 wt%) was examined for its reusability efficiency for Cd^{2+} sorption from aqueous solution. As presented in Table 10, the adsorption and desorption efficiencies of re-generated NM-WS-RH-AC for Cd(II) sorption were maintained between 77.14 - 78.58% and 61.18–62.74% respectively for consecutive four cycles. This result reveals a relatively equal adsorption-desorption efficiencies which shows excellent reusability of adsorbent with good stability. This could be attributed to the presence of magnetite binding the walnut shell and rice husk particles together to enhance adsorbent's stability nature towards Cd(II) removal from aqueous solution. This attribute makes NM-WS-RH-AC to be economically viable and proves its suitability as adsorbent for treatment of waste water.

3.5. Proposed adsorption mechanisms

For proper understanding of how Cd^{2+} was being removed from aqueous solution using NM-WS-RH-AC, it is necessary to propose the

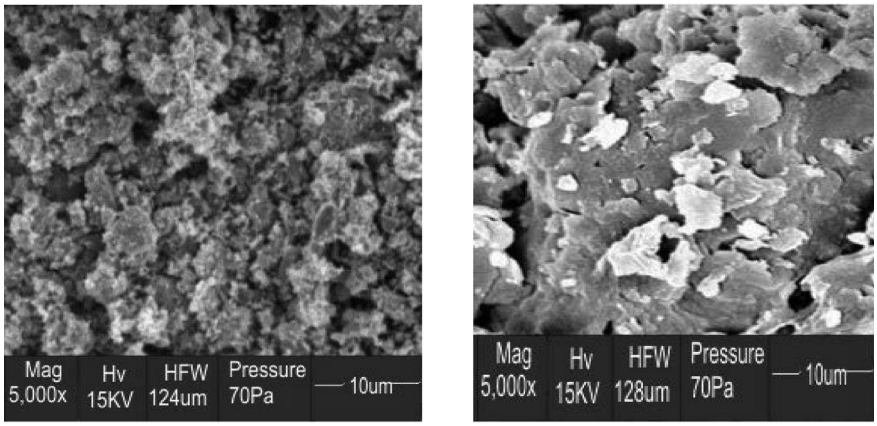

(a) (b)

Fig. 6. SEM image of NM-WS-RH-AC (a) before and (b) after Cd(II) sorption.

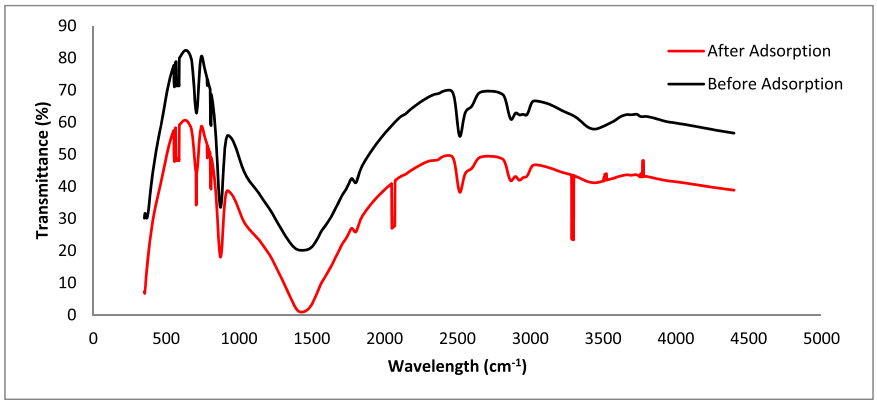

Fig. 7. FTIR spectra of NM-WS-RH-AC before and after Cd(II) adsorption.

Table 7
EDS analysis of NM-WS-RH-AC adsorbent before and after Cd(II) sorption.

Element	Wt (%) Before Adsorption	Wt (%) After Adsorption
Al	1.01	0.96
K	2.41	2.48
Ca	13.21	15
S	2.89	2.23
Si	21.2	19.11
O	15.24	9.52
H	3.03	1.51
Fe	38.85	36.22
Na	2.16	3.33
Cd	-	9.64

Table 8
Surface area, pore volume and pore diameter of RWS-RH, CWS-RH, NM-WS-RH-AC and CAC.

Characteristics	RWS-RH	CWS-RH	NM-WS-RH-AC	CAC
Surface area (m^2/g)	38.08	94.54	126.72	67.87
Total pore volume (cm^2/g)	0.0073	0.0932	0.0811	0.0108
Average pore diameter (Å)	2.77	3.31	4.18	2.88

Table 9
Textural properties of previous nanomagnetic activated carbons of parent materials used as adsorbent.

Nanomagnetic Activated Carbon of Materials	Surface area (m^2/g)	Total pore volume (cm^2/g)	Average pore diameter (Å)	Reference
Oil palm frond	700.00	0.3200	5.85	Zainol et al., (2017)
saponite clay	69.07	0.3058	17.66	Makarchuk et al., (2016)
kenaf core fiber	4.00	0.1128	28.39	Idan et al., (2018)
wood	101.51	0.0567	22.35	Sahu et al., (2009)
walnut shell-rice husk	126.72	0.0811	4.18	This study

Table 10
Adsorption-desorption efficiencies of regenerated NM-WS-RH-AC for Cd(II) sorption.

No of cycles	Adsorption Efficiency (%)	Desorption Efficiency (%)
1	78.58	62.74
2	77.81	61.35
3	77.02	61.18
4	77.14	61.92

reaction mechanism between the positively charged Cd^{2+} and existing negatively charged ions on NM-WS-RH-AC surface by binding electrostatic forces. The executed FTIR analysis has revealed presence of –OH, –NH and COO^- on adsorbent surface whose ionisation is a function of the Cd^{2+} solution pH by either gaining or losing a proton. The NM-WS-RH-AC surface becomes positively charged at low solution pH by gaining a proton. Thus, Eqs. (9), (10), and (11) exist.

$$\text{NM-WS-RH-AC} - \text{OH} + \text{H}^+ \rightarrow \text{NM-WS-RH-AC} - \text{OH}_2^+ \quad (9)$$

$$\text{NM-WS-RH-AC} - \text{NH} + \text{H}^+ \rightarrow \text{NM-WS-RH-AC} - \text{NH}_2^+ \quad (10)$$

$$\text{NM-WS-RH-AC} - \text{COOH} + \text{H}^+ \rightarrow \text{NM-WS-RH-AC} - \text{COOH}_2^+ \quad (11)$$

When the solution pH is very high, NM-WS-RH-AC surface becomes negatively charged by losing a proton as presented in Eqs. (12), (13), and (14).

$$\text{NM-WS-RH-AC} - \text{OH} + \text{OH}^- \rightarrow \text{NM-WS-RH-AC} - \text{O}^- + \text{H}_2\text{O} \quad (12)$$

$$\text{NM-WS-RH-AC} - \text{NH} + \text{OH}^- \rightarrow \text{NM-WS-RH-AC} - \text{N}^- + \text{H}_2\text{O} \quad (13)$$

$$\text{NM-WS-RH-AC} - \text{COOH} + \text{OH}^- \rightarrow \text{NM-WS-RH-AC} - \text{COO}^- + \text{H}_2\text{O} \quad (14)$$

Thus, electrostatic attractive forces favoured sorption of Cd^{2+} onto NM-WS-RH-AC surface when solution pH was high such that the proposed adsorption mechanisms could be presented as Eqs. (15), (16), and (17).

$$\text{NM-WS-RH-AC} - \text{O}^- + \text{Cd}^{2+} \rightarrow \text{NM-WS-RH-AC} - \text{O}^{-\cdots}\text{Cd} \quad (15)$$

$$\text{NM-WS-RH-AC} - \text{N}^- + \text{Cd}^{2+} \rightarrow \text{NM-WS-RH-AC} - \text{N}^{-\cdots}\text{Cd} \quad (16)$$

$$\text{NM-WS-RH-AC} - \text{COO}^- + \text{Cd}^{2+} \rightarrow \text{NM-WS-RH-AC} - \text{COO}^{-\cdots}\text{Cd} \quad (17)$$

4. Conclusion

In this study, an eco-friendly low-cost activated carbon adsorbent was prepared from walnut shell and rice-husk wastes via calcination and magnetization processes with the objective of using it to remove hazardous Cd(II) from aqueous solution. An efficiency of 78.58% at 2-level factorial design expert was revealed while optimum preparation conditions of 859.20 °C, 2.32 h, 2.54 and 5.56 wt% for calcination temperature, calcination time, SS-RH mixing ratio and magnetite loading were predicted respectively. Executed sensitivity analysis of model factors by both 2^k factorial design and ANN revealed calcination temperature as the most contributory factor enhancing NM-WS-RH-AC efficiency for Cd(II) sorption with significance of 44.87% and 44.82% respectively. However, average relative errors and R^2 values of 1.2931% and 4.806%; and 0.9967 and 0.9055 obtained respectively for developed ANN model with 4-9-1 architecture and 2-level factorial design expert revealed ANN

model as better prediction and optimization tool for Cd(II) sorption using NM-WS-RH-AC. SEM image revealed change in adsorbent textural and morphological structure after Cd(II) adsorption. FTIR revealed presence of –OH, –NH and COO^- groups on adsorbent surface. EDS showed Cd(II) was present in the adsorbent after adsorption. BET revealed increase in NM-WS-RH-AC surface area and average pore diameter due to magnetization. In conclusion, the prepared adsorbent is effective in removing Cd(II) from solution than commercial activated carbon with economically viable regeneration attribute.

Declarations

Author contribution statement

Lekan Popoola: Conceived and designed the experiments; Performed the experiments; Analyzed and interpreted the data; Contributed reagents, materials, analysis tools or data; Wrote the paper.

Funding statement

This research did not receive any specific grant from funding agencies in the public, commercial, or not-for-profit sectors.

Competing interest statement

The authors declare no conflict of interest.

Additional information

No additional information is available for this paper.

References

AbdurRahman, F.B., Akter, M., Abedin, M.Z., 2013. Dyes removal from textile wastewater using orange peels. Int. J. Sci. Technol. Res. 2, 2277–8616.

Akhtar, M.S., Swamy, M.K., Umar, A., Al Sahli, A.A., 2015. Biosynthesis and characterization of silver nanoparticlesfrom methanol leaf extract of Cassia didymobotyra and assessment of their antioxidant and antibacterialactivities. J. Nanosci. Nanotechnol. 15, 9818–9823.

Ali, I., 2012. New generation adsorbents for water treatment. Chem. Rev. 112 (10), 5073–5091.

Bailey, S.E., Olin, T.J., Bricka, M., Adrian, D.D., 1999. A review of potentially low-cost sorbents for heavy metals. Water Res. 33, 2469–2479.

Bhatnagar, A., Sillanpaa, M., 2010. Utilization of agro-industrial and municipal waste materials as potential adsorbents for water treatment: a review. Chem. Eng. J. 157, 277–296.

Bulut, Y., Aydin, H., 2006. A kinetics and thermodynamics study of methylene blue adsorption on wheat shells. Desalination 194 (1-3), 259–267. https://www.sciencedirect.com/science/article/pii/S0011916406003791.

Calvete, T., Lima, E.C., Cardoso, N.F., Dias, S.L.P., Pavan, F.A., 2009. Application of carbon adsorbents prepared from the Brazilian pine-fruit-shell for the removal of Procion Red MX 3B from aqueous solution-kinetic, equilibrium and thermodynamic studies. Chem. Eng. J. 155, 627–636.

Cao, C., Xiao, L., Chen, C., Shi, X., Cao, Q., Gao, L., 2014. In situ preparation of magnetic Fe_3O_4/chitosan nanoparticles via a novel reduction-precipitation method and their application in adsorption of reactive azo dye. Powder Technol. 260, 90–97.

Chatterjee, S., Chatterjee, T., Lim, S.R., Woo, S.H., 2011. Effect of the addition mode of carbon nanotubes for the production of chitosan hydrogel core-shell beads on adsorption of Congo red from aqueous solution. Bioresour. Technol. 102 (6), 4402–4409.

Chen, Y., Huang, B., Huang, M., Cai, B., 2011. On the preparation and characterization of activated carbon from mangosteen shell. J. Taiwan Inst. Chem. Eng. 42 (5), 837–842.

Ernhart, C.B., 1992. A critical review of low-level prenatal lead exposure in the human: 1. Effects on the fetus and newborn. Reprod. Toxicol. 6 (1), 9–19.

Fan, F., Qin, Z., Rong, W., 2012. Rapid removal of uranium from aqueous solutions using magnetic Fe_3O_4/SiO_2 composite particles. J. Environ. Radioact. 106, 40–46.

Garg, V.K., 2005. Removal of a basic dye from aqueous solution by adsorption using timber industry waste. Chem. Biochem. Eng. 19 (1), 75–80.

Garson, G.D., 1991. Interpreting neural network connection weights. Artif. Intell. Expert 6 (4), 47–51.

Giri, S.K., Das, N.N., Pradhan, G.C., 2011. Synthesis and characterization of magnetite nanoparticles using waste iron ore tailings for adsorptive removal of dyes from aqueous solution. Colloid. Surf. Physicochem. Eng. Asp. 389, 43–49.

Guimarães Gusmão, K.A., Alves Gurgel, L.V., Sacramento Melo, T.M., Gil, L.F., 2012. Application of succinylated sugarcane bagasse as adsorbent to remove methylene blue and gentian violet from aqueous solutions - kinetic and equilibrium studies. Dyes Pigments 92, 967–974.

Gupta, V., Moradi, O., Tyagi, I., Agarwal, S., Sadegh, H., Shahryari-Ghoshekandi, R., Makhlouf, A., Goodarzi, M., Garshasbi, A., 2016. Study on the removal of heavy metal ions from industry waste by carbon nanotubes: effect of the surface modification: a review. Crit. Rev. Environ. Sci. Technol. 46 (2), 93–118.

Gupta, V.K., Nayak, A., 2012. Cadmium removal and recovery from aqueous solutions by novel adsorbents prepared from orange peel and Fe_2O_3 nanoparticles. Chem. Eng. J. 180, 81–90.

Henretig, F.M., 2006. In: Flomenbaun, N.E., Goldfrank, L.R., Hoffman, R.S., Howland, M.A., Lewin, N.A., Nelson, L.S. (Eds.), Goldfrank's Toxicologic Emergencies, eighth ed. McGraw-Hill, New York, pp. 1308–1324.

Ho, Y.S., 2004. Kinetic modeling and equilibrium studies during cadmium biosorption by dead *Sargassum* sp. biomass. Bioresour. Technol. 91 (3), 249–257.

Hu, S., Guan, Y., Wang, Y., Han, H., 2011. Nano-magnetic catalyst KF/CaO–Fe_3O_4 for biodiesel production. Appl. Energy 88 (8), 2685–2690.

Huang, J., Cao, Y., Liu, Z., Deng, Z., Tang, F., 2012. Efficient removal of heavy metal ions from water system by titanate nanoflowers. Chem. Eng. J. 180, 75–80.

Idan, I.J., Luqman, C.A., Thomas, S.Y.C., Siti, N.A.B.M.J., 2018. Equilibrium, kinetics and thermodynamic adsorption studies of acid dyes on adsorbent developed from kenaf core fiber. Adsorpt. Sci. Technol. 36 (1–2), 694–712.

Khataee, A.R., Kasiri, M.B., 2011. Modeling of biological water and wastewater treatment processes using artificial neural networks. Clean (Weinh) 39 (8), 742–749.

Khlifi, R., Hamza-Chaffai, A., 2010. Head and neck cancer due to heavy metal exposure via tobacco smoking and professional exposure: a review. Toxicol. Appl. Pharmacol. 248 (2), 71–88.

Korotkova, T.G., Ksandopulo, S.J., Donenko, A.P., Bushumov, S.A., Danilchenko, A.S., 2016. Physical properties and chemical composition of the rice husk and dust. Orient. J. Chem. 32 (6), 3213–3219.

Krishna Mohan, G.V., Naga Babu, A., Kalpana, K., Ravindhranath, K., 2017. Removal of chromium (VI) from water using adsorbent derived from spent coffee grounds. Int. J. Environ. Sci. Technol.

Krishnaa, D., Padma Sree, R., 2013. Removal of chromium from aqueous solution by custard apple (Annona Squamosa) peel powder as adsorbent. Int. J. Appl. Sci. Eng. 11 (2), 171–194.

Lasheen, M.R., El-Sherif, I.Y., El-Wakee, S.T., Sabry, D.Y., El-Shahat, M.F., 2017. Heavy metals removal from aqueous solution using magnetite Dowex 50WX4 resin nanocomposite. JMES 8 (2), 503–511.

Lima, E.C., Royer, B., Vaghetti, J.C.P., Brasil, J.L., Simon, N.M., dos Santos Jr., A.A., Pavan, F.A., Dias, S.L.P., Benvenutti, E.V., Silva, E.A., 2007. Adsorption of Cu(II) on *Araucaria angustifolia* wastes: determination of the optimal conditions by statistic design of experiments. J. Hazard Mater. 140, 211–220.

Ma, W., Ya, F-Q., Han, M., Wang, R., 2007. Characteristics of equilibrium, kinetics studies for adsorption of fluoride on magnetic-chitosan particle. J. Hazard Mater. 143 (1), 296–302.

Machado, F.M., Bergmann, C.P., Fernandes, T.H.M., Lima, E.C., Royer, B., Calvete, T., Fagan, S.B., 2011. Adsorption of Reactive Red M-2BE dye from water solutions by multi- walled carbon nanotubes and activated carbon. J. Hazard Mater. 192 (3), 1122–1131.

Makarchuk, O.V., Dontsova, T.A., Astrelin, I.M., 2016. Magnetic nanocomposites as efficient sorption materials for removing dyes from aqueous solutions. Nanoscale Res. Lett. 11, 161.

Mall, I.D., Srivastava, V.C., Kumar, G.V.A., Mishra, I.M., 2006. Characterization and utilization of mesoporous fertilizer plant waste carbon for adsorptive removal of dyes from aqueous solution. Colloid. Surf. Physicochem. Eng. Aspects 278, 175–187.

Miralles, N., Valderrama, C., Casas, I., Martinez, M., Florido, A., 2010. Cadmium and lead removal from aqueous solution by grape stalk wastes: modeling of a fixed-bed column. J. Chem. Eng. Data 55, 3548–3554.

Mittal, A., 2006. Adsorption kinetics of removal of a toxic dye, Malachite Green, from wastewater by using hen feathers. J. Hazard Mater. 133 (1), 196–202.

Moreno-Castilla, C., Álvarez-Merino, M.A., López-Ramón, M.V., Rivera-Utrilla, J., 2004. Cadmium ion adsorption on different carbon adsorbents from aqueous solutions: effect of surface chemistry, pore texture, ionic strength, and dissolved natural organic matter. Langmuir 20, 8142–8148.

Nasr, M., Moustafa, M., Seif, H., El Kobrosy, G., 2012. Application of artificial neural network (ANN) for the prediction of EL-AGAMY wastewater treatment plant performance- Egypt. Alex Eng. J. 51 (1), 37–43.

Nassar, N., 2010. Rapid removal and recovery of Pb (II) from wastewater by magnetic nanoadsorbents. J. Hazard Mater. 184, 538–546.

Novopashin, S., Serebryakova, M., Khmel, S., 2015. Methods of magnetic fluid synthesis: a review. Thermophys. Aeromechanics 22, 397–412.

Ozcan, A., Oncu, E.M., Ozcan, A.S., 2006. Adsorption of acid blue 193 from aqueous solutions onto DEDMA-sepiolite. J. Hazard Mater. 129 (1-3), 244–252.

Panneerselvam, P., Morad, N., Tan, K.A., 2011. Magnetic nanoparticle (Fe_3O_4) impregnated onto tea waste for the removal of nickel (II) from aqueous solution. J. Hazard Mater. 186 (1), 160–168.

Park, H.J., McConnell, J.T., Boddohi, S., Kipper, M.J., Johnson, P.A., 2011. Synthesis and characterization of enzyme-magnetic nanoparticle complexes: effect of size on activity and recovery. Colloids Surfaces B Biointerfaces 83 (2), 198–203.

Popoola, L.T., 2016. Expert System Design and Control of Crude Oil Distillation Column Using Artificial Neural Network Based Monte Carlo Simulation. PhD Thesis. Chemical and Polymer Engineering, Lagos State University.

Popoola, L.T., 2019. Characterization and adsorptive behaviour of snail shell-rice husk (SS- RH) calcined particles (CPs) towards cationic dye. Heliyon 5, e01153.
Popoola, L.T., Aderibigbe, T.A., Yusuff, A.S., Munir, M.M., 2018. Brilliant green dye adsorption onto composite snail shell–rice husk: adsorption isotherm, kinetic, mechanistic and thermodynamics analysis. Environ. Qual. Manag. 1–16.
Popoola, L.T., Susu, A.A., 2014. Application of artificial neural networks based Monte Carlo simulation in the expert system design and control of crude oil distillation column of a Nigerian refinery. Adv. Chem. Eng. Sci. 4, 266–283.
Popuri, S.R., Vijaya, Y., Boddu, V.M., Abburi, K., 2009. Adsorptive removal of copper and nickel ions from water using chitosan coated PVC beads. Bioresour. Technol. 100 (1), 194–199.
Ranasinghe, R.A.T.M., Jaksa, M.B., Kuo, Y.L., Pooya Nejad, F., 2017. Application of artificial neural networks for predicting the impact of rolling dynamic compaction using dynamic cone penetrometer test results. JRMGE 9, 340–349.
Rao, M.M., Ramesh, A., Rao, G.P.C., Seshaiah, K., 2006. Removal of copper and cadmium from the aqueous solutions by activated carbon derived from *Ceiba pentandra* hulls. J. Hazard Mater. 129 (1), 123–129.
Rehman, R., Mahmud, T., Irum, M., 2015. Brilliant green dye elimination from water using *Psidium guajava* leaves and *Solanum tuberosum* peels as adsorbents in environmentally benign way. J. Chem. 2015, 126036. www.hindawi.com/journals/jchem/2015/126036/abs.
Robinson, T., 2002. Removal of dyes from an artificial textile dye effluent by two agricultural waste residues, corncob and barley husk. Environ. Int. 28, 29–33.
Sadegh, H., Ali, G.A.M., Gupta, V.K., Makhlouf, A.S.H., Shahryari-ghoshekandi, R., Nadagouda, M.N., Sillanpa, M., Megie, E., 2017. The role of nanomaterials as effective adsorbents and their applications in wastewater treatment. J. Nanostruct. Chem. 7, 1–14.
Sahu, J.N., Acharya, J., Meikap, B.C., 2009. Response surface modeling and optimization of chromium(VI) removal from aqueous solution using tamarind wood activated carbon in batch process. J. Hazard Mater. 172 (2-3), 818–825. www.sciencedirect.com/science/article/pii/S0304389409011832.
Sharma, Y., Srivastava, V., Singh, V., Kaul, S., Weng, C., 2009. Nanoadsorbents for the removal of metallic pollutants from water and wastewater. Environ. Technol. 30 (6), 583–609.
Singh, A., Tripathi, A., Dutta, N.N., 2017. Optimisation of brilliant green dye removal efficiency by electrocoagulation using artificial neural networking and comparison with response surface methodology. Int. J. Eng. Sci. Comput. 2 (2), 10588–10594.
Singh, K.K., Talat, M., Hasan, S., 2006. Removal of lead from aqueous solutions by agricultural waste maize bran. Bioresour. Technol. 97, 2124–2130.
Sublet, R., Simonnot, M.O., Boireau, A., Sardin, M., 2003. Selection of an adsorbent for lead removal from drinking water by a point-of-use treatment device. Water Res. 37 (20), 4904–4912.
Swamy, M.K., Akhtar, M.S., Mohanty, S.K., Sinniah, U.R., 2015. Synthesis and characterization of silver nanoparticles using fruit extract of Momordica cymbalaria and assessment of their in vitro antimicrobial,antioxidant and cytotoxicity activities. Spectrochim. Acta A Mol. Biomol. Spectrosc. 151, 939–944.
Tan, I.A., Ahmad, A.L., Hameed, B.H., 2008. Adsorption of basic dye on high-surface-area activated carbon prepared from coconut husk: equilibrium, kinetic and thermodynamic studies. J. Hazard Mater. 154 (1), 337–346.
Tanyildizi, M.S., 2011. Modeling of adsorption isotherms and kinetics of reactive dye from aqueous solution by peanut hull. Chem. Eng. J. 168 (3), 1234–1240. https://www.sciencedirect.com/science/article/pii/S1385894711001896.
Tunc, Ö., Tanaci, H., Aksu, Z., 2009. Potential use of cotton plant wastes for the removal of remazol black B reactive dye. J. Hazard Mater. 163 (1), 187–198. https://www.sciencedirect.com/science/article/pii/S0304389408009722.
Wan Ngah, W.S., Teong, L.C., Hanafiah, M.A.K.M., 2011. Adsorption of dyes and heavy metal ions by chitosan composites: a review. Carbohydr. Polym. 83 (4), 446–1456.
Wannahari, R., Sannasi, P., Nordin, M.F.M., Mukhtar, H., 2018. Sugarcane bagasse derived nano-magnetic adsorbent composite (SCB-NMAC) for removal of Cu^{2+} from aqueous solution. ARPN J. Eng. Appl. Sci. 13 (1), 1–9.
Yao, S., Liu, Z., Shi, Z., 2014. Arsenic removal from aqueous solutions by adsorption onto iron oxide/activated carbon magnetic composite. J. Environ. Health Sci. Eng. 12, 1–8.
Yazdani, M., Bahrami, H., Arami, M., 2014. Preparation and characterization of chitosan/feldspar biohybrid as an adsorbent: optimization of adsorption process via response surface modeling. Sci. World J.J. 2014, 370260, 1-13.
Zainol, M.M., Asmadi, M., Amin, N.A.S., 2014. Impregnation of magnetic particles on oil palm shell activated carbon for removal of heavy metal ions from aqueous solution. J. Teknol. 72 (1), 7–11.
Zainol, M.M., Asmadi, M., Amin, N.A.S., 2017. Preparation and characterization of impregnated magnetic particles on oil palm frond activated carbon for metal ions removal. Sains Malays. 46 (5), 773–782.
Zhou, Y., Branford-White, C., Nie, H., Zhu, L., 2009. Adsorption mechanism of Cu^{2+} from aqueous solution by chitosan-coated magnetic nanoparticles modified with α-ketoglutaric acid. Colloids Surfaces B Biointerfaces 74, 244–252.